Supporting Information

Saito et al. 10.1073/pnas.1620612114

Assisting Structures for Wing Folding

SEM observations identified various microdevices in the body of insects, which confer versatile functions (28–31). Previous studies reported the existence of the microspicules and trichia on the abdominal terga, underside of the elytra, and surface of hindwings in various species of beetles (2, 4). These microstructures are believed to fulfill functions for the elytra/abdomen in interlocking in the resting position and supporting wing folding. In the beetles with complex foldable hindwings, represented by rove beetles (Staphylinidae) and ladybird beetles, the patch-like structures dense with microspicules are commonly observed on the tergites, known as wing-folding spicule patches (2). Fig. S2 shows the abdominal tergite and wing-folding spicule patches in *Coccinella septempunctata*. These patches are positioned on tergites 2–6. Each plate contains a pair of patches in the median region, and tergites 5 and 6 contain additional patches laterally. Tergite 7 appears to contain no patch-like structures but is instead uniformly covered by smaller spicules. It is evident that the positions of these patches are related to the resting position of the hindwings. The spicule directions of the patches on tergites 4–6 that are positioned just under the folded hindwings have complex patterns. The patches are considered to fulfill functions to increase (or decrease) friction for a particular direction on the abdominal terga and to bind wing membranes in the proper position in midfolded shapes. By the presence of these wing-folding spicule patches, simple up-and-down movements of the abdomen can achieve the complex folding patterns with two transverse folding lines. In regard to the undersurface of the elytra, our SEM observations identified no observable microstructures, except for the microspicules in the center of the basal position and lateral side. Considering the position of these spicules, they are believed to be the elytra interlocking structures (31) and probably have no function for supporting wing folding.

Rigid Foldability in Origami Crease Patterns

Rigid foldability (15, 16) is an important property in origami crease patterns. If the given crease pattern is rigid-foldable, it means that the facets and fold lines can be replaced with rigid panels and ideal hinges, respectively, and the origami pattern can be folded without facet deformations. Under rigid-foldable conditions where origami can be described by geometric restrictions, researchers have proposed several methods for simulating the folding process (32, 33). The rigid foldability of a given crease pattern can be investigated by the mechanical degree of freedom (DOF). If the crease pattern has no hole and there is no redundant constraint, the DOF is expressed by the following equation (16):

$$\mathrm{DOF} = N_{\mathrm{E}} - 3N_{\mathrm{V}}, \qquad \textbf{[S1]}$$

where N_{E} is the total number of fold lines and N_{V} is the total number of vertices. When DOF ≥ 1, the crease pattern is determined to be rigid-foldable. Fig. 3*A* has 14 folding lines and five vertices; thus, the DOF is calculated as −1. Therefore, this pattern is not rigidly foldable in general, and its folding/unfolding process should include the elastic deformations of facets.

Crease Patterns and Supporting Structures in Beetle Hindwings

Although beetles show enormous diversity in body size and shape and there are large differences in the crease patterns and shapes of the supporting structures in hindwings among species, it is possible to discuss the following general tendency (1, 8, 9, 34). Large-sized beetles, such as rhinoceros and other scarab beetles (Scarabaeidae), require intense wing flapping to gain the lifting force to counterbalance their heavy weight; therefore, they have generally developed thick veins that confer high rigidity and strength in wings. The wing-folding mechanisms in these types of beetles are inevitably simple and, in most cases, use a single folding along the longitudinal direction (1, 8). Additional small transverse folding lines are found in the wing apexes of some of these beetles; however, they separate the movements of the main folding lines and do not contribute to the storing efficiency. On the other hand, small-sized beetles, such as ant-loving beetles (Staphylinidae: Pselaphinae), require little rigidity in hindwings and have relatively thin veins with sufficient flexibility, which are beneficial for compact wing folding. For example, some species of ant-loving beetles fold the hindwings using accordion-like patterns with six or seven transverse folding lines (1). Some groups of rove beetles fold the hindwings using right-to-left asymmetrical crease patterns, thereby achieving highly compact wing folding (5). From a standpoint of engineering applications, the high rigidity and strength of wings in large-sized beetles are attractive; however, the storing efficiency is not high. The highly compact wing folding found in small-sized beetles is very interesting; however, the weakness in the mechanical properties of the wings limits the possible applications. Ladybird beetles are believed to occupy an intermediate position between these two groups.

Finite Element Analysis of the Tape Spring-Like Vein

To demonstrate the structurally reinforcing properties of the tape-spring vein, the commercial finite element analysis (FEA) software ANSYS was used to simulate the static bending test. The finite element model was made from the surface data of SV_2, which was extracted from the results of micro-CT scanning (Fig. 2*A*). A total of 5,809 shell elements were used to model the SV_2 vein. Per the micro-CT results, the cell thickness was set to 0.015 mm, approximately the average thickness of the vein. The cuticle, the main material for hindwings, is known to exhibit a very wide range of mechanical properties depending on the citin fiber and moisture content (35). It is difficult to measure Yong's module of the vein cuticle from a living ladybird beetle. This study used Yong's module of the general wing cuticle (6.0 GPa), as described by Vincent and Wegst (35). For simplified discussion, the isotropic linear elastic element was used. The basal edge line of the numerical model was completely fixed, and 5.0×10^{-4} N of a uniformly distributed load (nearly equal to the weight of a ladybird beetle) was applied on the top surface in the vertical direction (−Z in Fig. S3). For comparison, the same flat-shaped plate with an equal weight was simulated using the same material and boundary conditions. Fig. S3 shows the calculated result. Maximum displacements are 0.068 mm (tape spring) and 0.7 mm (flat plate); therefore, the tape spring cross-section has about 11-fold higher bending stiffness than the flat-shaped vein. With respect to the strength of cuticle, there are data reporting that the tensile strength of a locust femoral cuticle is 60–200 MPa, which is about 1–5% of the stiffness (35). According to the FEA result, the maximum stress of the tape spring model is 15.2 MPa (about 0.5% of the stiffness). Therefore, it can be said that the tape spring vein possesses sufficient strength to withstand the same level of the static load as the body weight. Actual wing veins are not uniform solid plates but have complex inner structures, and their material composition also exhibits anisotropic and nonlinearity properties. Therefore, the above value should only be used as a reference. Although further experimental investigation is required to determine accurate mechanical properties of the hindwings, these results show that tape spring veins have large structural reinforcement properties.

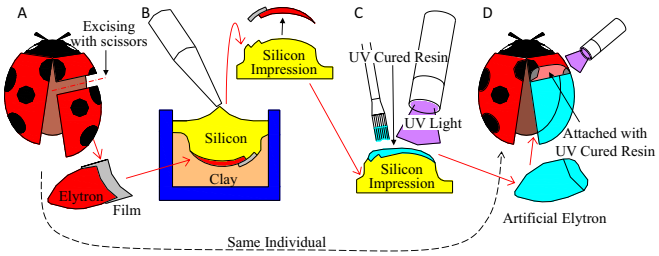

Fig. S1. Schematic representation of the transplant operation. (*A*) Ladybird beetle was anesthetized using carbon dioxide gas, and two-thirds of its apical right elytron was excised using scissors. To construct the connecting portion, a small-sized thin film was attached on the top surface of the cut plane on the excised elytron. (*B*) Elytron and film are mounted on the clay with the ventral surface up, and two-part silicone (Sildefit wash-XS; SHOFU Co., Ltd.) was applied. After curing (5 min at 25 °C), the elytron and film were peeled off from the impression. (*C*) UV-cured resin (Craft arrange clear; CHEMITECH, Inc.) was applied in a thin layer on the impressions using a brush. After curing by UV light, the transparent acrylic elytron was fabricated. (*D*) Artificial elytron was adhered to the apices of the right wing of the original ladybird beetles using the UV-cured resin.

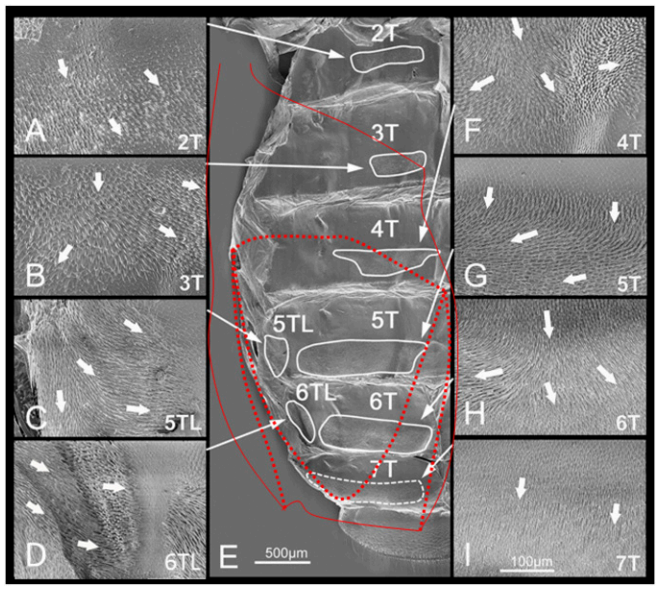

Fig. S2. Abdominal tergites and wing-folding spicule patches in *C. septempunctata*. These figures were micrographed using SEM. (*A–D* and *F–I*) Wing-folding spicule patches. (Magnification: 1,000×.) (*E*) Abdominal tergites. (Magnification: 200×.) The red dotted lines show the position of the folded hindwing in a resting state. 2T to 7T, abdominal tergites 2–7; 5TL and 6TL, abdominal tergites 5 and 6, lateral patch. The white arrows show the directions of the spicules. The SEM sample was dissected from the insect specimen, uncoated, and treated using the nanosuits method (36). The sample was observed and photographed using a digital microscope system (KEYENCE VHX-2000 + VHX-D510) under an accelerating voltage of 1.2 kV.

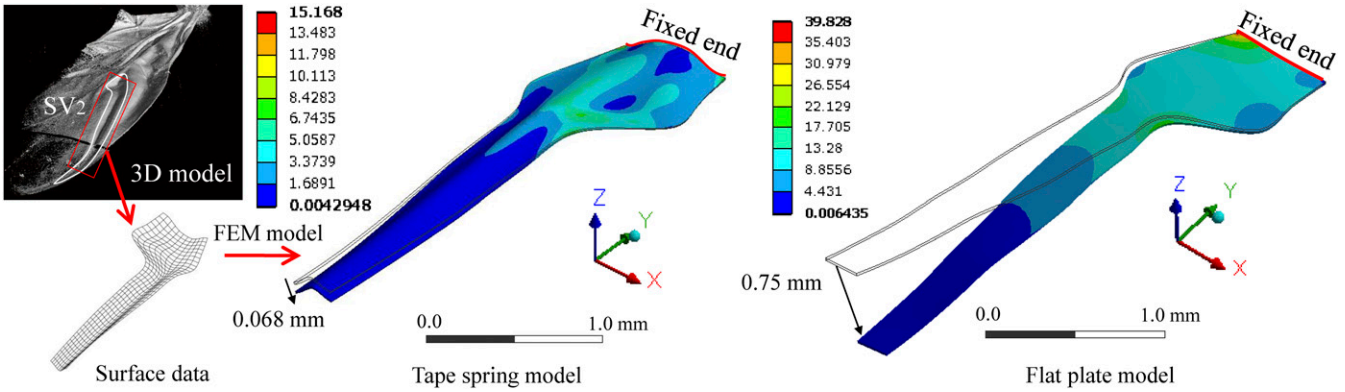

Fig. S3. Simulated results of the bending test in the tape spring vein. Commercial finite element analysis software, ANSYS, was used to simulate the static bending test. (*Left* and *Center*) Tape spring model was made from the surface data of SV_2, which was extracted from the results of the micro-CT scans. A total of 5,809 shell elements were used to model the SV_2 vein. For comparison, the flat plate model (5,105 shell elements) was made from the side edges of the tape spring model (*Right*). The isotropic linear elastic element (Yong's module = 6.0 GPa, Poisson's ratio = 0.3) was used in both models. Basal edge lines of the numerical models were completely fixed, and a 5.0×10^{-4} N uniformly distributed load (almost equal to the weight of a ladybird beetle) was applied on the top surface along the $-z$ axis. The color bars illustrate the equivalent stress (measured in megapascals).

Movie S1. Wing-deploying motion of a ladybird beetle imaged with a high-speed camera. The hindwing deployment in the takeoff motion was very fast and completed within 0.1 s from the fully folded state.

Movie S1

Movie S2. Wing-folding motion of a ladybird beetle imaged with a high-speed camera. Ladybird beetles are known to use their elytra and abdomen for folding. The transplantation of the artificial acrylic elytron enables a detailed observation of these wing-folding techniques.

Movie S2

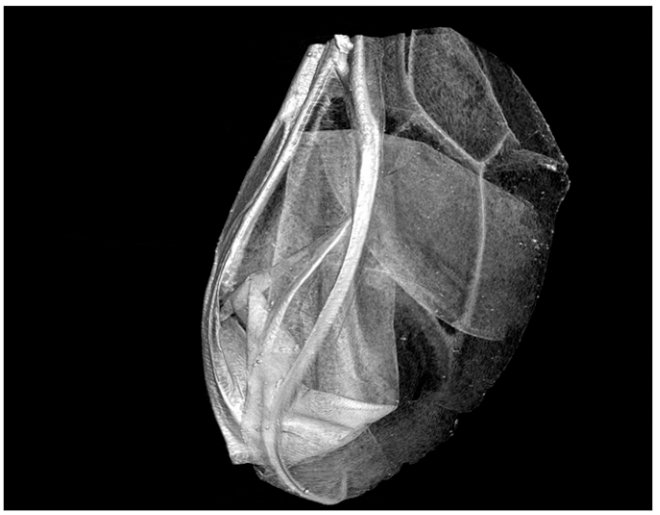

Movie S3. Translucent image of the folded hindwing in *C. septempunctata* reconstructed by the result of the micro-CT scan. The wing is not folded into a flattened shape but has slightly open angles to fit into the storage space between the elytron and abdomen.

Movie S3